ELSEVIER

0958-9465(95)00043-7

Cement & Concrete Composites **18** (1996) 47–59

0958-9465/96/$15.00

Deterioration of Concrete Due to Reinforcement Steel Corrosion

J. G. Cabrera

CEMU, University of Leeds, Leeds LS2 9JT, UK

(Received 16 June 1995; accepted 4 January 1996)

Abstract

Steel corrosion in concrete leads to cracking, reduction of bond strength, reduction of steel cross section and loss of serviceability. Reinforced concrete undergoing corrosion does not only give the appearance of poor performance, but can in extreme cases, lose its structural integrity.

Numerical relations to assess the loss of serviceability due to steel reinforcement corrosion are scanty, thus data to relate the rate of corrosion to cracking and loss of bond strength are necessary.

This paper uses laboratory data to investigate the effects of corrosion rate on cracking and bond strength loss.

It also examines the influence of fly ash on the rate of reinforcement corrosion.

The laboratory data is used to develop numerical models to predict:

(a) rate of corrosion from the width and intensity of cracking,
(b) bond stress from corrosion rate, and
(c) serviceability loss from corrosion rate.

Key words: Concrete, reinforcement, cracking, corrosion, serviceability, fly ash

INTRODUCTION

The basic problem associated with the deterioration of reinforced concrete due to corrosion is not that the reinforcing itself is reduced in mechanical strength, but rather that the products of corrosion exert stresses within the concrete which cannot be supported by the limited plastic deformation of the concrete, and the concrete therefore cracks.[1] This leads to a weakening of the bond and anchorage between concrete and reinforcement which directly affects the serviceability and ultimate strength of concrete elements within a structure.

The assessment of the loss of serviceability of reinforced concrete is made on the basis of models or the measurement of corrosion rates. The most known conceptual model is the Tuutti model[2] which involves two stages; the initial stage or initiation stage and the propagation stage which involves active corrosion. Authors have used variations of this conceptual model to determine service life of concrete. Browne[3] for example, used a diffusion model for prediction of the remaining life of in-service reinforced concrete structures exposed to chloride laden environments. He and many others used a threshold value of chloride concentration to determine the remaining service life.

Measurements of corrosion currents of steel reinforcement have been used by Andrade and co-workers[4–6] for estimating the remaining service life. Corrosion current is converted to loss of steel section and this is used as the threshold to determine remaining service life.

These approaches however do not really relate the 'loss of structural serviceability' to the rate of corrosion or to the state of active steel corrosion. Studies to develop models to assess the structural serviceability loss are few[7–9] and therefore it is important to continue these studies in order to provide structural engineers with the appropriate tools for the repair and maintenance of reinforced concrete structures. It is also important to improve knowledge on the relationship between rate of corrosion and cracking. Visual inspections of concrete struc-

tures are based, on the first instance, in recording the signs of surface distress among which cracking due to reinforcement corrosion is the most important.

This paper presents a summary of laboratory investigations carried out at the Civil Engineering Materials Unit (CEMU), University of Leeds, as part of a large study on the *structural consequences of steel corrosion on reinforced concrete structures*. In particular the paper discusses the following:

(1) The relationship between corrosion rate and crack pattern and intensity obtained from experiments using small concrete beams subjected to accelerated corrosion.
(2) The relationship between corrosion rate and loss of structural serviceability from measurements of bond strength, cracking and deflection of concrete beams.
(3) The influence of cement type is evaluated using a normal portland cement (OPC) and a pozzolanic cement composed of 70% normal portland cement and 30% pulverised fuel ash (PFA).

MATERIALS

The cement used in this investigation was normal portland cement conforming to BS 12:1991. The fly ash was a low Ca ash typical of ashes produced in the UK and was used to prepare a pozzolanic cement by replacing 30% of normal portland cement with the fly ash. The proportion of cement and aggregate in the mixtures was calculated using the minimum porosity method.[10] The concrete mixtures consisted of 1:2·3:3·5 cement, sand and gravel, respectively (proportion by weight). The cement content was 325 kg/m^3 and the water cement ratio was 0·55. Sodium chloride was added to the mixture to accelerate the corrosion process, the amount added was equivalent to 2% Cl^- (percent based on the cementitious content).

High yield deformed bars, grade 460 complying with the requirements of BS 4449:1988 were used for the experimental work. The bars were cleaned and polished before placement into the concrete specimens. In order to insulate the tensile reinforcement bars of the beam specimens from the rest of the steel cage, the corner of the stirrups were coated with an insulating polymer plastic applied at 300°C.

PREPARATION OF SPECIMENS

Crack characteristics study

The test specimens consisted of 100 mm × 300 mm × 200 mm reinforced concrete slabs. Three preformed steel bars were embedded 180 mm into the concrete specimens. The protruding ends of the bars at the concrete surfaces and the top 20 mm of the bars in the concrete were sealed with plastic tape and silicon to minimise corrosion in these areas, therefore, only 160 mm length of bars were exposed to concrete. Concrete specimens were also made with additional reinforcement placed across the main bars. This reinforcement consisted of two 8 mm diameter deformed bars (see Fig. 1). This part of the programme was designed to study the effect of cement type, bar diameter, cover thickness and cross bar inclusion on the intensity, extent and pattern of cracking. Table 1 shows the details of the experimental parameter and type of specimens.

Pullout tests study

The pullout tests were carried out on 150 mm concrete cubes with 12 mm diameter reinforcing bar centrally embedded in the cube. In order to

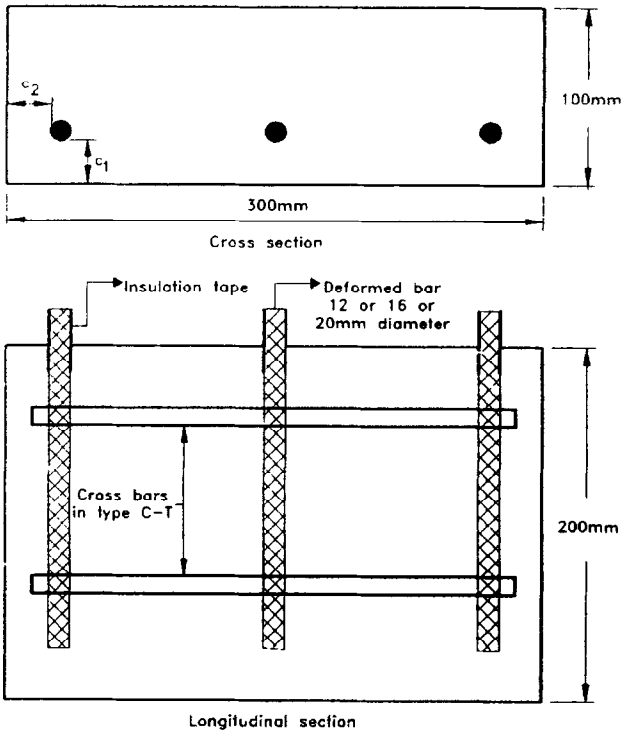

Fig. 1. Geometry of the specimens used in the study.

Table 1. Type of specimens and experimental parameters

Group	*Type*	*Bar size (mm)*	*Type of bar cage*	*Cement type*	c_1 *(mm)*	c_2 *(mm)*	*Aim of test*
A	A-12	12	one way	OPC	20	44	Effect of bar diameter
	A-16	16	one way	OPC			
	A-20	20	one way	OPC			
B	B-OPC	12	one way	OPC	20	20	Effect of cement type
	B-PFA	12	one way	PFA			
C	C-O	12	one way	OPC	30	30	Effect of cross bars
	C-T	12	two way	OPC			

*Slab types B-OPC and C-O also compared for cover thickness effect.
**c_1=cover thickness from longitudinal face (Fig. 1).
***c_2=cover thickness from side face.

ensure that the bond slip failure would dominate over other types of failure such as anchorage splitting and yielding of the steel reinforcement, only a short length of reinforcement was bonded to concrete. The embedment length chosen was 4 × the bar diameter.

Beam tests study

These specimens were reinforced concrete beams having a cross section of 125 × 160 mm with two different embedment lengths and shear spans. In 'series I' beams the embedment length was 384 mm in accordance with the requirements of BS 8110 1985 to ensure that flexural failure would dominate over other types of failure. In 'series II' beams the length of embedment was 190 mm, to ensure that bond slip failure would dominate. The beams were essentially of the type described in the report of ACI committee 208. In these beams, recesses of 100 mm length were made to expose the bars under the concentrated loads and to set up the instrumentation for measuring steel strains and loaded-end slips.

All beams had two 12 mm deformed bars at the bottom and two 10 mm plain bars at the top with links of 8 mm plain bars as web reinforcement along the shear spans at 40 mm spacing. The outside portions of the reinforcing bars at the end of each beam beyond the support were covered by plastic tubes to eliminate bond in the extended part of the specimens.

CURING AND EXPOSURE CONDITIONS

After casting, the concrete specimens were kept in their moulds covered with damp hessian and polythene at room temperature (20°C) for 24 h. Then they were demoulded and kept under the same conditions for 3 days. The specimens were then stored at 35°C and 45% RH until the age of 28 days. The 28 day cured specimens were partially immersed to a depth equal to the concrete cover in a 5% NaCl solution. Specimens for control were immersed in tap water.

All specimens were kept partially immersed for 3 days to obtain uniform moisture distribution in the immersed part of the specimen. After this period the specimens were either tested or subjected to accelerated corrosion and then tested.

METHODS OF TESTING

Corrosion acceleration and testing

Figure 2 shows schematically the electrochemical system used. The stainless steel plate immersed in the solution is used as counter electrode and a potentiostat is set in such a way that the reinforcing steel acts as an anode and the counter electrode as a cathode. A voltage of 3 V versus saturated calomel electrode (SCE) was impressed through the system to accelerate corrosion.

The current was recorded at increasing exposure times and cracking of the specimens was visually observed and recorded. The electrical resistivity of the specimens was measured at the same times.

The amount of corrosion on the steel of the pullout specimens was found by the gravimetric weight-loss method and in the steel of the beams by calculation using Faraday's law.

Pullout tests

Pullout tests were carried out using an Instron testing machine under monotonic static load.

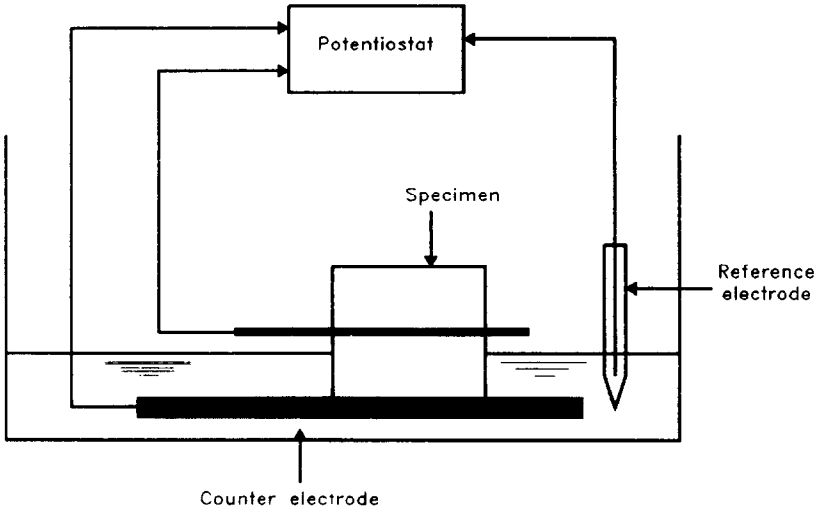

Fig. 2. Schematic representation of the electrochemical system.

Three dial gauges were used to measure the values of slip at both ends. At the loaded end of the specimens, two dial gauges were fixed to a steel bar that was fastened to the sides of the concrete by bolts. Figure 3 shows the testing arrangement.

In determining the slip at the loaded end, the gauge readings at each increment were corrected for the elongation of the reinforcing bar with the distance between the fixed point of the gauge and the surface of the concrete.

Beam flexure tests

The beam specimens were tested as simply supported beams with two concentrated loads using an Instron testing machine. Figure 4(a) and (b) show the testing arrangements.

For series II beams, strain in the tensile reinforcement within the opening in the concrete was measured with electrical resistance strain gauges. The strain gauges were fixed on the bottom side of the bars after the specimens had been cured. Both free end and loaded end slips of the bars were measured with 0·002 mm scale dial gauges. The beams were tested under monotonic increasing load up to failure, in order to observe their static flexural behaviour.

RESULTS AND DISCUSSION

Measurements of crack width and intensity

The measurement of crack width was carried out using an Ultra Lomara 250b microscope. Two values of crack width are reported, i.e. the

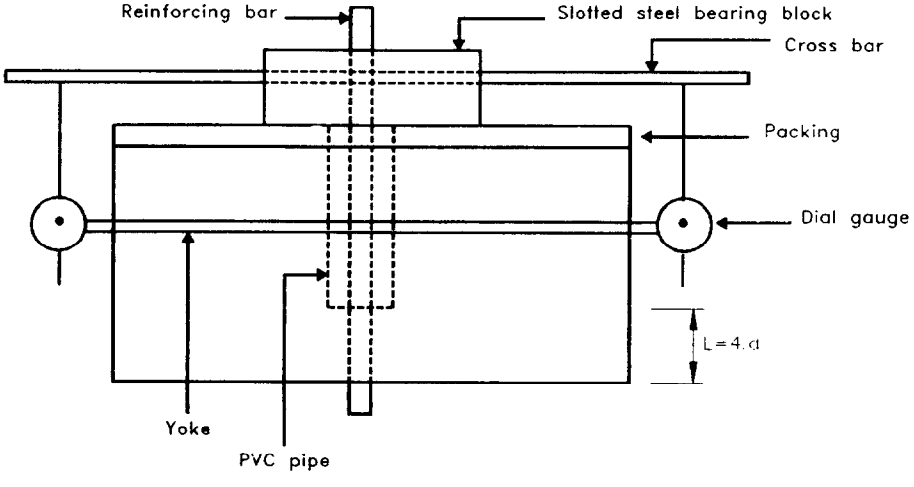

Fig. 3. Arrangement for the pullout test.

maximum crack width on the longitudinal side which was found to be approximately equal to the maximum crack width on the top surface (cross section) of a slab, and the average crack width.

To quantify crack intensity, this was expressed as the total length of cracks on the top surface of the concrete slab (cross section) divided by the surface area of the same cross section, which as seen in Fig. 1, was 300 cm^2. In all the slabs, the cracks developed parallel to the bars. In the case of slabs with one way bars, the direction of cracks were vertical and in slabs with two way bars, the cracks appeared in the horizontal direction. The differences in crack pattern on the top surface of the slabs were not significant except for the cracks in the slab with cross bars. These slabs exhibited only one crack emanating from the steel bars and following the direction of the cross bars as shown in Fig. 5.

The corrosion current and resistance at 1, 16 and 28 days acceleration for all specimens are presented in Table 2. An increase in the bar diameter caused the corrosion current to increase. This is expected since larger bar size had higher surface area and lower electrical resistance. Larger bar diameter caused lower corrosion resistance before cracking. At later age, after cracking, particularly at 28 days, the resistance values of the bars of different sizes were approximately the same. Comparing the measured resistance before cracking, there was a reduction of 59, 56 and 47%, respectively. This then shows that the reduction in resistance is larger in smaller bars than in larger bars.

As expected, the slabs with 20 mm cover thickness (B-OPC) showed higher corrosion current and lower resistance than the slabs with 30 mm cover thickness (C-O). Because of the smaller cover thickness and lower electrical resistance the diffusion path for the chloride ions was the shortest. The cover thickness therefore, was the dominant variable even after cracking.

Table 2 also reveals that the corrosion current of specimens made with normal portland cement was much higher than that of fly ash. At all ages, the corrosion current of normal portland cement specimens was more than 8 times that of the fly ash specimens.

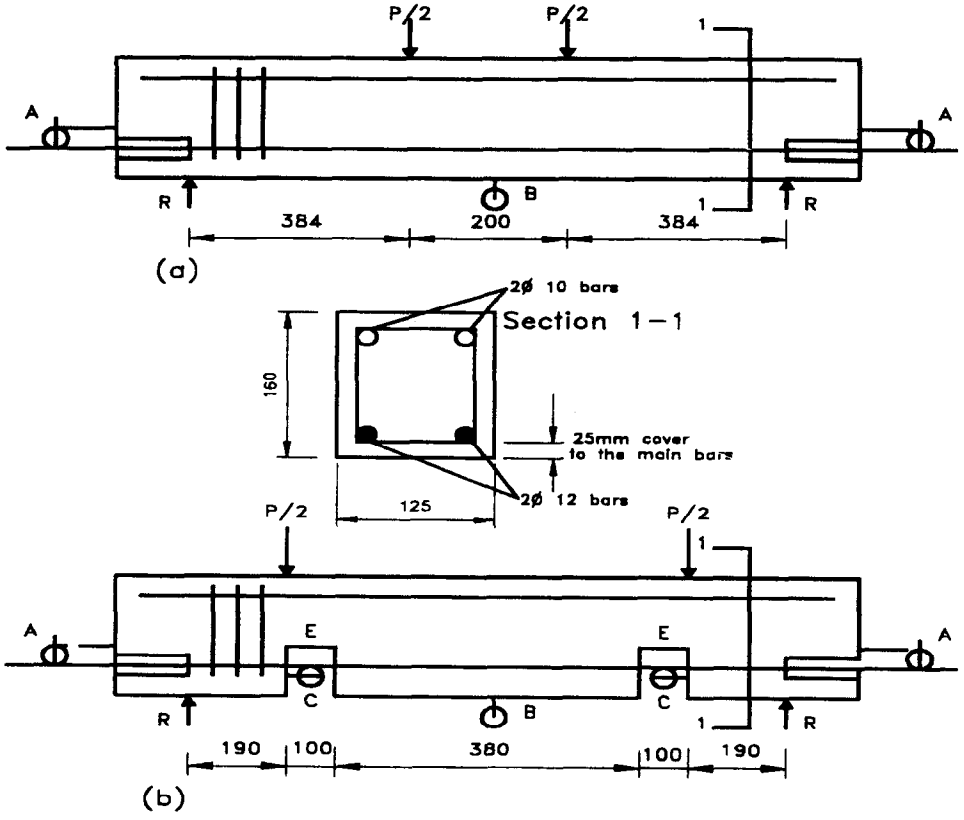

Fig. 4. (a) Arrangement for beam tests, Series I: (b) Arrangement for beam tests, Series II (all dimensions in mm). Notation: A — dial gauges of the free end slip measurement, B — dial gauges for measurement of the mid span deflection, C — dial gauges for the loaded end slip measurement, E — electrical strain gauges for steel strain measurement, P — applied load, R — reaction at supports.

Fly ash slabs cracked in a period which was, on average, 5 times more than the cracking period for normal portland cement slabs. The resistance of fly ash slabs was more than 7 times that of the resistance of normal portland cement slabs. The high values of fly ash concrete resistance have been discussed in previous papers.[12,13]

The results of corrosion current measurements of two way reinforced slabs are not

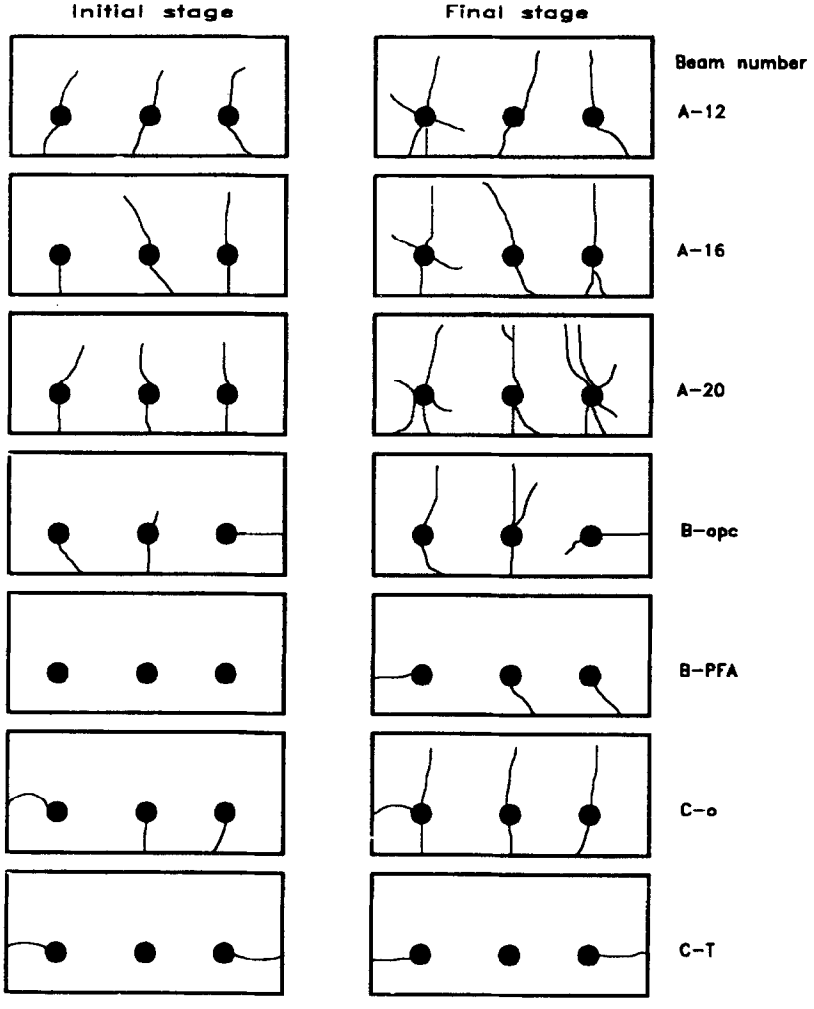

Fig. 5. Crack patterns caused by corrosion of the reinforcing steel.

Table 2. Corrosion current and resistance

Slab type	*Number of days under accelerated corrosion*					
	1 day		*16 days*		*28 days*	
	Current (mA)	*Resistance (Ω)*	*Current (mA)*	*Resistance (Ω)*	*Current (mA)*	*Resistance (Ω)*
A-12	19	133	40·5	81·5	54·5	54·5
A-16	22·5	118·5	45·5	69·5	58·0	52·5
A-20	24·5	99·5	49·5	67·5	64·0	53·5
B-OPC	17·5	143	43·0	75·0	59·0	50·0
B-PFA	2·5	1084	4·6	712	6·15	481·0
C-O	14·5	198	30·5	106	39·5	82·0

Table 3. Corrosion weight loss and crack intensity at the end of the experiment

Slab type	*Measured reinforcement weight loss (%)*	*Calculated reinforcement weight loss (%)*	*Measured weight loss (g/cm^2)*	*Crack intensity (mm/cm^2)*
A-12	17·73	19·69	0·463	0·93
A-16	12·80	12·50	0·393	0·95
A-20	6·76	8·78	0·345	1·02
B-OPC	19·21	20·15	0·480	0·74
B-PFA	3·55	2·02	0·045	0·20
C-O	13·48	13·77	0·320	0·99

presented because the cage was connected and direct readings cannot be used for comparison.

A summary of the results of weight loss and crack intensity at the end of the experiment (28 days) is shown in Table 3.

Influence of corrosion on crack pattern and crack width

When making visual inspections of concrete structures, the major signs of distress due to corrosion which are normally reported correspond to crack pattern, intensity and width of cracks. If these are numerous then the visual inspection is followed by testing to ascertain the extent of corrosion of the reinforcing steel. The testing programmes carried out for this purpose are not only time consuming but very expensive, therefore data to link crack pattern, crack intensity or crack width to the amount of corrosion may be potentially very useful to determine policies of maintenance, repair or demolition of concrete structures.

There is relatively scant information with regard to the prediction of crack pattern caused by the expansion of reinforcement corrosion in concrete.[11] Maruyama *et al.*[14] proposed a model for prediction which indicates that the pattern of cracking is predominantly influenced by the cover thickness, however, Ergatoudis *et al.*[15] have shown that cracking pattern is dependent not only on cover thickness, but also on the overall position of the steel bar within the depth, width and height of the concrete element. They have proposed three models of cracking pattern, according to these the cracking pattern of the slabs tested in this work corresponds mainly to models 1 and 2. The cracking patterns at the initial and final stages of the experiment are shown in Fig. 5.

The first crack caused by corrosion appeared as expected through the shortest path between steel bar and concrete surface i.e. from the bar to the surface cover. The second crack appeared at an angle of 10° against the direction of the first crack, this crack direction corresponds to model 1 and is very close to model 2, proposed in Ref. 15.

The crack width measured and expressed either as average crack width or as a maximum crack width was related to the weight loss due to the corrosion of the steel bars expressed in g/cm^2. The resultant relations were then compared with the estimations of crack width which were calculated as follows.

(a) The increase of bar diameter due to the corrosion of the steel was calculated according to the following formula:

$$\Delta d = \{(\sqrt{d^2 + 4W_l d/\rho}) - d\}/2 \qquad (1)$$

where:

d=diameter of steel bar (cm)
Δd=increase in bar diameter due to corrosion (cm)
W_l=steel weight loss g/cm^2
ρ=density of corrosion product

The crack width was then calculated using the formula proposed in Ref. 15.

$$W_C = 4\Delta d\{[(c_1 + d/2)/(c_2 + d/2)] \sin\theta + \cos\theta\} \sin\theta \qquad (2)$$

where:

W_c=crack width (cm)
c_1 c_2=distances from the bar to the cover surface and the surface perpendicular to it (see Fig. 1) (cm)
θ=angle between the direction of first crack and the direction of the second crack.

Table 4 presents the data of average crack width, maximum crack width and calculated crack width together with the corresponding measured values of steel weight loss W_l. Observation of this Table shows that the calculated values predict reasonably the measured values (either average or maximum crack width).

The prediction is quite accurate when the corrosion product density is equal to 3·9 g/cm^3, that is when the volume increases due to the oxidation reaction is two times that of the original steel and when the total weight loss per unit areas does not exceed 0·2 g/cm^2. This is quite understandable since the mechanism of cracking is related to the initial build up of pressure up to the tensile strength of the concrete followed by accelerated increase of the crack width and subsequent release of pressure by flow of the reaction product.

Loss of bond from pullout tests

For each load level, bond stress is calculated as the average stress between reinforcing bar and surrounding concrete along the embedded portion of the bar. Comparisons of bond strength at different levels of corrosion can be made in terms of a limiting slip or in terms of maximum load. A method to determine the critical bond stress f_{cb}, from the bond stress–slip relationship has been used by a number of investigators.[16,17] In this method the critical bond stress (f_{cb}) is taken as the lower value of the bond stress corresponding to a loaded-end slip (S'_l) of 0·25 mm and a free end slip (S'_f) of 0·051 mm.

The relationships between average bond stress and the values of free end slip are shown in Figs 6 and 7 and the relationship between bond strength and percent corrosion is shown in Fig. 8. These results clearly illustrate that bond strength increases with corrosion rate up to a maximum after which increasing corrosion causes a significant reduction of bond strength.

On the basis of ultimate bond stress, the relative bond strength of normal portland cement specimens exhibiting 12·6% corrosion, was reduced to only 23·8% of that for the control specimen with no corrosion. The reduction of bond resistance is even higher if the calculation is made on the basis of critical bond stress.

Table 4. Measured (maximum and average) and calculated crack widths and increase in bar diameter for the specimens used in the study
W_m=maximum crack width (mm), W_a=average crack width (mm)

Parameter	*Specimen type*					
	A-12	*A-16*	*A-20*	*B-OPC*	*B-PFA*	*C-O*
W_l (g/cm^2)	0·048	0·04	0·036	0·04	0·004	0·031
	0·108	0·094	0·083	0·10	0·008	0·072
	0·167	0·148	0·131	0·16	0·013	0·12
	0·231	0·203	0·179	0·23	0·020	0·17
	0·463	0·394	0·345	0·48	0·045	0·32
Δd (cm)	0·012	0·01	0·009	0·01	0·001	0·008
	0·027	0·024	0·21	0·025	0·002	0·018
	0·041	0·037	0·033	0·040	0·003	0·03
	0·056	0·050	0·045	0·056	0·005	0·04
	0·109	0·095	0·085	0·113	0·011	0·08
W_c (mm)	0·08	0·06	0·06	0·07	0·00	0·06
	0·18	0·16	0·14	0·18	0·00	0·13
	0·27	0·25	0·22	0·28	0·02	0·21
	0·37	0·33	0·30	0·40	0·04	0·28
	0·73	0·63	0·57	0·81	0·08	0·57
W_m (mm)	0·06	0·08	0·11	0·09	0·00	0·10
	0·13	0·18	0·30	0·13	0·00	0·19
	0·28	0·41	0·43	0·20	0·02	0·26
	0·35	0·49	0·53	0·34	0·06	0·33
	0·38	0·56	0·56	0·39	0·11	0·41
W_a (mm)	0·04	0·05	0·06	0·05	0·00	0·06
	0·09	0·11	0·19	0·11	0·00	0·11
	0·21	0·22	0·31	0·19	0·02	0·21
	0·27	0·33	0·37	0·26	0·04	0·29
	0·29	0·43	0·46	0·31	0·06	0·35

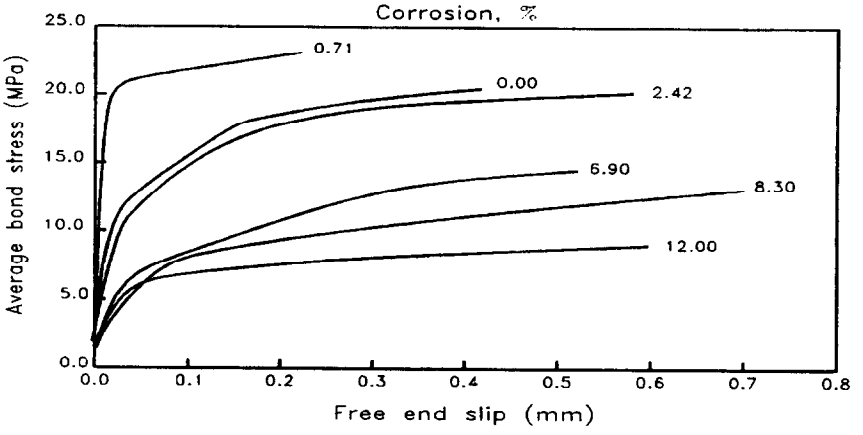

Fig. 6. Comparison of bond behaviour for pullout normal portland cement specimen with different levels of corrosion.

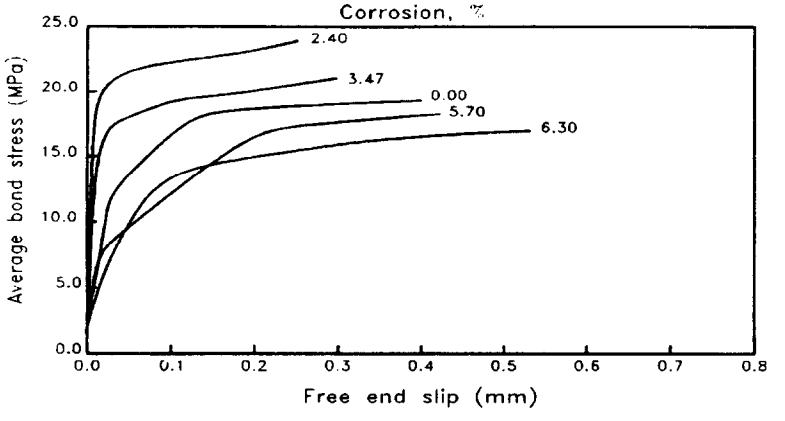

Fig. 7. Comparison of bond behaviour for pullout fly ash specimen with different levels of corrosion.

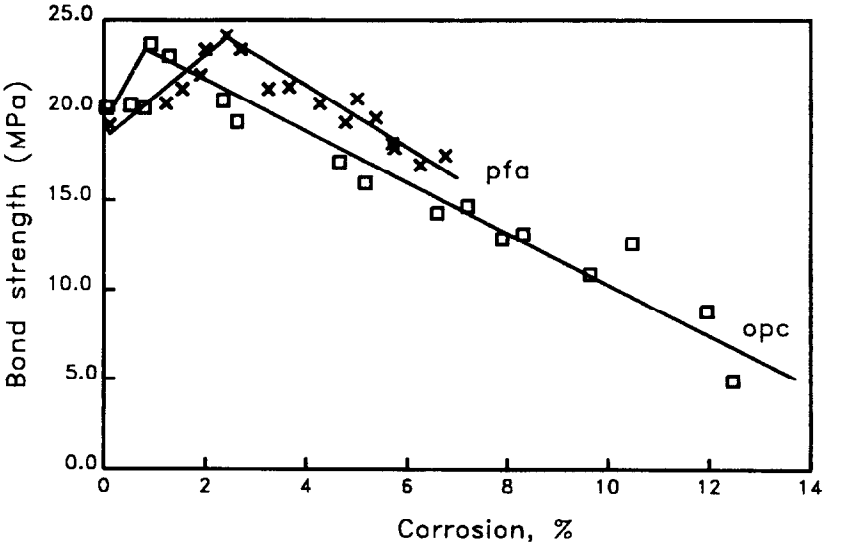

Fig. 8. Effect of corrosion on bond strength.

At the same corrosion percentage the fly ash concrete specimens exhibit higher bond resistance than the normal portland cement concrete specimens. For example, 6·5% corrosion caused 27% loss of bond strength in the normal portland cement specimens but only 14% loss in the fly ash concrete specimens. It is also important to point out that to induce the same level of corrosion in fly ash concrete than in normal portland cement concrete the time required was 3 times as much in fly ash concrete.

The improved bond resistance of fly ash concrete is attributed to the very low level of damage observed in the fly ash concrete. Only 2 specimens were cracked. One of them cracked at 42 days of accelerated corrosion and the other after 46 days. These specimens were subjected to an additional period of accelerated corrosion to obtain 6·3 and 6·9% corrosion.

The higher bond resistance of fly ash concrete is a result of the lower corrosion rate of the reinforcing bars. The rate of corrosion is a function of the availability of oxygen, moisture and the resistivity of the concrete.[12] The changes of electrical resistivity with age of the normal portland cement and fly ash concrete specimens are shown in Fig. 9. These results show clearly that the effect of fly ash on the electrical resistance of concrete is significant as has been shown previously by Cabrera.[13]

Numerical relations to calculate the reduction of bond strength caused by the level of corrosion can be obtained by regression analysis of the experimental results shown in Fig. 6, disregarding the values where corrosion causes an increase in bond strength.

The equation obtained for normal portland cement and fly ash are:

$$f_{bo}=23{\cdot}478-1{\cdot}313C\ (r^2=0{\cdot}960) \quad (3)$$

$$f_{bp}=26{\cdot}133-1{\cdot}341C\ (r^2=0{\cdot}909) \quad (4)$$

where:

f_{bo}=bond strength of normal portland cement concrete (MPa)

f_{bp}=bond strength of fly ash concrete (MPa)

C=corrosion (%)

r^2=correlation coefficient.

Influence of corrosion rate on beam deflection

The beams of series I (Fig. 4(a)) failed by yielding of the bars. The beams of series II (Fig. 4(b)) failed with excessive slip at the free end of the bars. Detailed results of bond stress versus corrosion rate have been reported elsewhere,[8] therefore in this paper the analysis presented deals with the deflection behaviour of the corroded beams.

In the limit state design of concrete structures deflection is one of the limit states which the design has to satisfy, to ensure serviceability of the structure. One of the most important aspects of bond performance is its influence on deflection and crack development.

Values of deflection at mid span of beams are shown in Figs 10 and 11. The relations were plotted up to the maximum observed values before failure. They show clearly that corrosion has significant influence on deflection.

Numerical relations to calculate the increases in deflection caused by corrosion are expressed

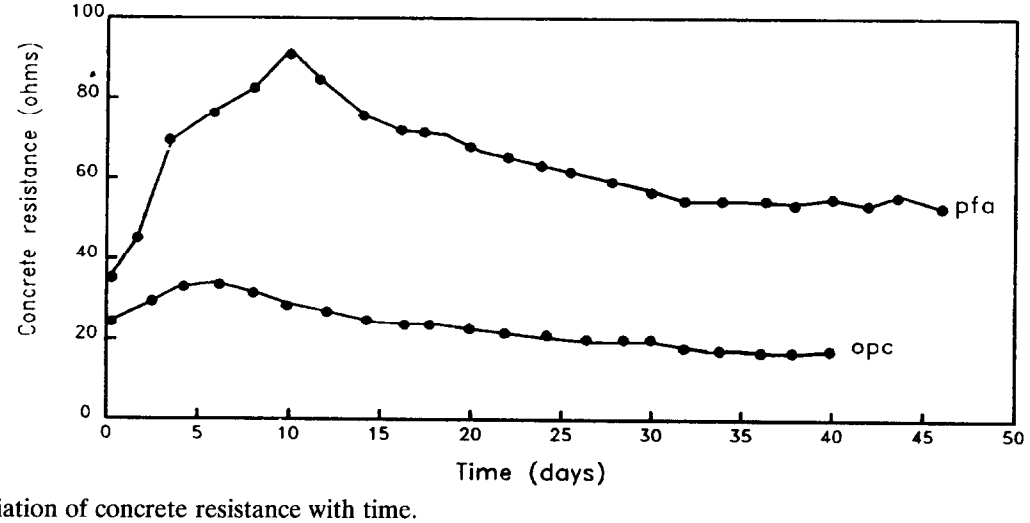

Fig. 9. Variation of concrete resistance with time.

in terms of deflection ratio versus corrosion percentage. The deflection ratio is the ratio of the deflection of the corroded beam divided by the deflection of the non-corroded beam loaded to the service load. The service load is defined as the ultimate load multiplied by 0·6.

Figure 12 shows these relations. Numerical expressions were obtained by simple linear regression analysis. Equation (5) corresponds to the normal portland cement concrete and eqn (6) to the fly ash concrete.

$$Dr = 1{\cdot}002 + 0{\cdot}050C \quad (r^2 = 0{\cdot}960) \tag{5}$$

$$Dr = 0{\cdot}943 + 0{\cdot}046C \quad (r^2 = 0{\cdot}936) \tag{6}$$

where:

Dr=deflection ratio
C=corrosion %
r^2=correlation coefficient.

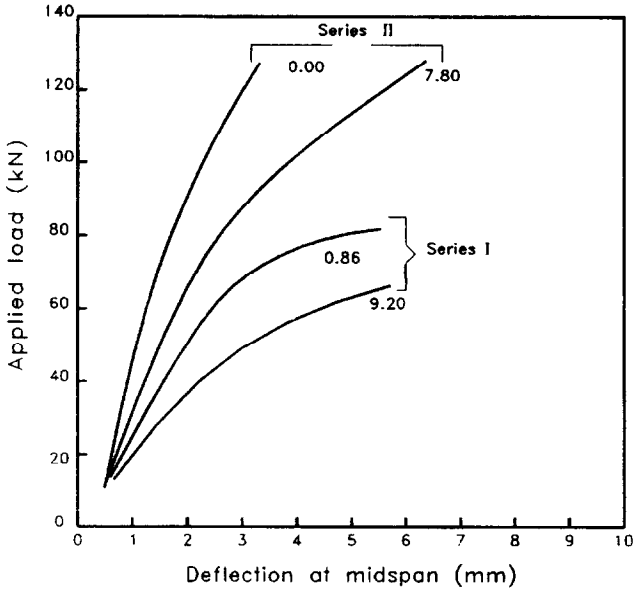

Fig. 10. Typical load vs deflection relationships for normal portland cement concrete beams.

CONCLUSIONS

From the experimental work carried out in this study and the application of theoretical predictive models, the following conclusions are offered.

(1) The results show that there is an inverse relation between steel bar cover and degree of corrosion. Crack intensity increases with increasing depth of cover and this can be numerically related to the degree of corrosion expressed as weight loss per unit area.
(2) Cracking pattern of slabs can be satisfactorily predicted using available models[9]

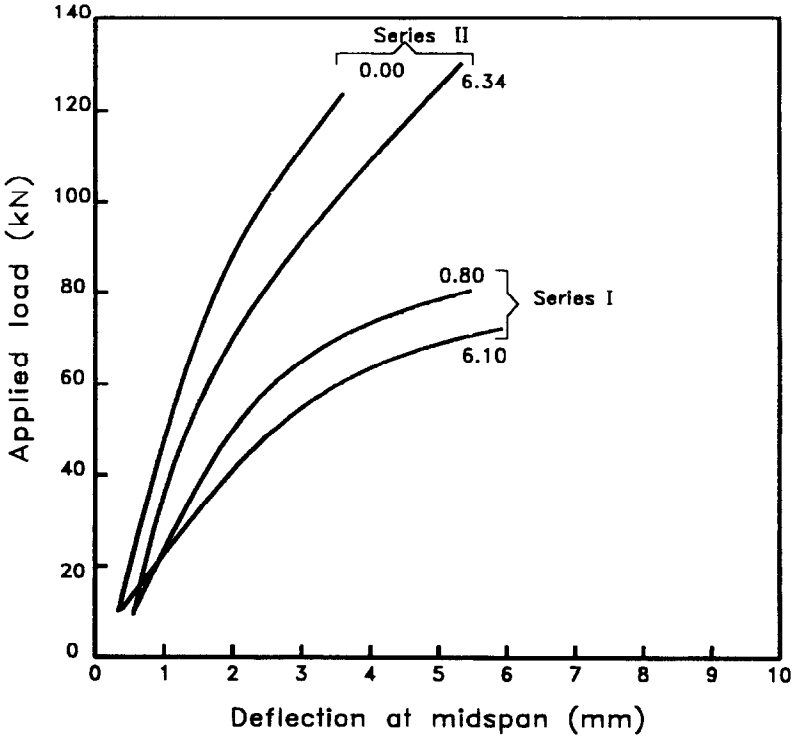

Fig. 11. Typical load vs deflection relationships for fly ash concrete beams.

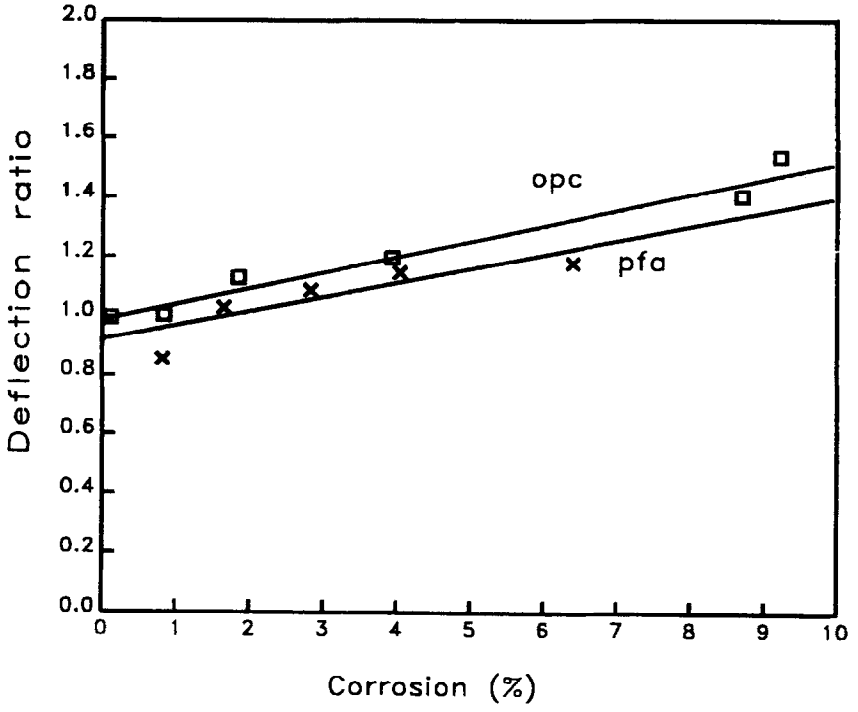

Fig. 12. Deflection ratio vs corrosion relationships for series I beams.

and crack widths can be approximated with acceptable degree of accuracy. Reasonable predictive models to estimate the corrosion rate from crack width measurements are presented.

(3) The bond strength measured in pullout specimens is significantly affected by the level of corrosion. Statistically significant relations to evaluate the effect of corrosion on bond strength are presented.

(4) Corrosion caused significant increases in the value of mid span deflection. When the corrosion level reached 9%, the beam deflection increased 1·5 times the deflection of the non-corroded beam.

Fly ash concrete exhibited better resistance to corrosion damage than normal portland cement concrete. The reduced level of corrosion in fly ash concrete is attributed to the higher resistivity of this concrete.

REFERENCESS

1. Slater, J.E., Magnitude of the problem. ASTM. STP 818, *Corrosion of Metals in Association with Concrete*, pp. 5–9, 1983.
2. Tuutti, K., *Corrosion of Steel in Concrete*. Swedish Cement and Concrete Research Institute, 1982.
3. Browne, R. D., Mechanisms of corrosion of steel in concrete, In *Concrete in Relation to Design, Inspection, and Repair of Offshore and Coastal Structures*. ACI SP-65, pp. 169–204, 1980.
4. Andrade, C., Alonso, C., Gonzales, J. A. & Rodriguez, J., Remaining service life of corroding structures, *IABSE Report 57/1, Durability of Structures*, pp. 359–364, 1989.
5. Andrade, C., Alonso, C. & Gonzales, J. A., An initial effort to use the corrosion rate measurements for estimating rebar durability, ASTM STP, *Corrosion Rates of Steel in Concrete*, pp. 29–37, 1990.
6. Andrade, C., Alonso, C. & Gonzales, J. A., Approach to the calculating of the residual life in corroding concrete reinforcement based on corrosion intensity values, *9th European Congress on Corrosion: Life Time Expectancy of Materials and Constructions*, Vol. 2, Ultrect, The Netherlands, 1989.
7. Al-Sulaimani Kaleemullah, M. Basunbul, I. A. Rasheeduzzafar. Influence of corrosion and cracking on bond behaviour and strength of reinforced concrete members. *Journal of the American Concrete Institute. Structural Journal*, **87** (1990) 220–231
8. Cabrera, J.G., Ghoddoussi, P. The effect of reinforcement corrosion on the strength of the steel concrete bond. *Proceedings of the International Conference on Bond in Concrete*, pp. 10/11–10/24, Riga, Latvia, 1992.
9. Rodriguez, J., Ortega L. M. & Garcia, A. M., Assessment of structural elements with corroded reinforcement. *Proc. of the International Conference on Corrosion and Corrosion Protection of Steel in Concrete.*, Vol. 1, pp. 171–185, 1994.
10. Cabrera, J. G., Design of concrete for minimum porosity. Concrete Research Seminar, Leeds, 1985.
11. C. Alonso & C. Molina, F.J. Cover cracking as a function of bar corrosion. Part I — Experimental test. *Materials and Structures*, **26** (1993) 453–464
12. Cabrera, J.G. & Ghoddoussi, P. The influence of pulverised fuel ash on the resistivity and rate of corrosion of reinforced concrete. Durability of Concrete. ACI. **145** (1994) 229–244

13. Cabrera, J.G. *The Use of Pulverised Fuel Ash to Produce Durable Concrete*. Institution of Civil Engineers, Thomas Telford, London, p. 164, 1985.
14. Maruyama, K., Takaoka, Y., Shimizu, K. & Nakada, Y. Cracking behaviour of concrete due to corrosion of reinforcing bars. *Transactions of the Japan Concrete Institute*. **11** (1989) 163–170
15. Ergatoudis, J., Beeby, A. W. & Cabrera, J. G., Prediction of crack pattern and crack width due to corrosion of reinforced steel in concrete. Submitted to *Magazine of Concrete Research*.
16. American Society for Testing and Materials: ASTM-A775M-86 Standard specification for epoxy-coated reinforcing bars. ASTM, 1986.
17. Marshall, A. L., *Marine Concrete*. Blackie and Son Ltd, pp. 230–235, 1.